The 8th European Congress on Computational Methods in Applied Sciences and Engineering
ECCOMAS Congress 2022
5-–9 June 2022, Oslo, Norway

DEVELOPMENT OF A 3D VISCO-ELASTIC MODEL FOR WOOD UNDER LARGE DEFORMATIONS

RAÚL LAZO-MOLINA, CARLOS FELIPE GUZMÁN, JUAN CARLOS PINA, ERICK I. SAAVEDRA FLORES AND SERGIO J. YANEZ

Civil Engineering Department, Faculty of Engineering
University of Santiago of Chile (USACH), Chile
e-mail: cf.guzman@usach.cl, obrasciviles.usach.cl

Key words: Wood, Visco-elasticity, Large deformations

Abstract. Some of the most frequently observed phenomena in structural materials are creep and relaxation. Both are associated with time-dependent behavior and dissipative rheological variables. In the case of wood, long-term creep can produce excessive deformation and instability problems by magnifying short-term deflections. Also, wood presents changes in its mechanical properties due to its hygroscopy, so that moisture appears as an important parameter to be considered. A priori, it is known that the moisture content in wood cells and the angle of microfibrils are parameters that directly affect the overall cell stiffness. With this information, material physics hypotheses can be elaborated to develop a constitutive model in large deformations to predict phenomena such as creep and relaxation in the medium and/or long term. The microstructure of the cell wall can be represented through a model of fiber-reinforced composite material originally developed for biomaterials such as arteries and fibrous tissues. Where the anisotropic character is conferred by the distribution of the fibers within the isotropic matrix of the material. This work aims to adapt these models to represent the mechanical behavior of the wood cell with faithful representation of its microstructure. FEniCS is used for the numerical implementation of the material. In this paper the validations, current status, conclusions, and perspectives of this research are presented.

1 INTRODUCTION

The mechanical properties of wood cell are determined by the features of its cell wall. Figure 1 shows an arrangement of wood cells and the sub-layers that compose their wall. Two main walls are highlighted: the primary layer (P) and the secondary layer. The latter is composed of the following sub-layers: outer layer (S_1), middle layer (S_2), and inner layer (S_3). The cell wall matrix is composed mainly of hemicellulose and lignin. In each cell wall sub-layer there are microfibrils, a polymeric structure composed of a cellulose core in a matrix of lignin and hemicellulose. The microfibrils are arranged in the matrix of each sub-layer with a certain orientation and angle (MFA) with respect to the longitudinal axis, forming a spiral distribution providing a high tensional strength to the cell. Therefore, the structure of the wood cell is a natural composite material reinforced with microfibrils.

According to Dinwoodie (2000), the primary wall P presents a random distribution of microfibrils without specific lamellation or angles. In the S_1 wall, microfibrils are arranged in 4-6

concentric lamellae with alternating left-right orientations, and angles between 50°-70°. The S_2 wall, the thickest, microfibrils are arranged in 30-150 lamellae with rightward orientation and angles between 10-30 degrees. Finally, the S_3 wall is patterned by varying angles between 60-90 degrees, in few sub-layers with alternating orientations as in the S_1 wall. Anisotropic behavior, tensile strength, and failure morphology of wood cell are related to the microfibrils angle (MFA). In order to study the anisotropic viscoelasticity of the wood cell, fiber-reinforced

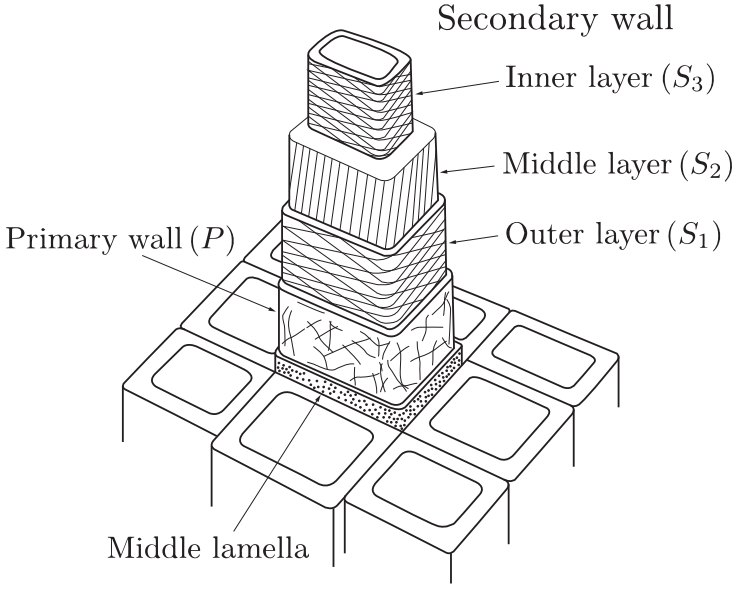

Figure 1: Cell arrangement and microstructure (adapted from Dinwoodie, 2000).

composite models originally proposed for biological materials such as arteries are used, assuming quasi-incompressible behavior for the wood cell.

2 NUMERICAL MODEL

In the following, the general framework will be described starting from the proposal of Holzapfel et al. (2000) to describe first the hyperelastic behavior of the material, and then extend to viscoelasticity. Then, a free energy function Ψ is considered whose additively separated parts represent the volumetric Ψ_{vol} and deviatoric $\overline{\Psi}_{\text{iso}}$ contributions of the isotropic matrix. The deviatoric contribution of the fibers $\overline{\Psi}_{\text{aniso}}$, to add the anisotropy behavior, depends on the orientation of the fibers through a directional vector a_0 for a single fiber arragement:

$$\Psi\left(\mathbf{C}, a_0\right) = \Psi_{\text{vol}}\left(J\right) + \overline{\Psi}_{\text{iso}}\left(\overline{\mathbf{C}}\right) + \overline{\Psi}_{\text{aniso}}\left(\overline{\mathbf{C}}, a_0\right), \tag{1}$$

where $\mathbf{C}$ is the right Cauchy-Green strain tensor, and $\overline{\mathbf{C}}$ the modified deviatoric version calculated with the Jacobian J as $\overline{\mathbf{C}} = J^{-2/3}\mathbf{C}$. A classical hyperelastic model from the isotropic theory can be used to model the matrix. To represent the mechanical response of the fibers, the Holzapfel-Gasser-Ogden (HGO) (Holzapfel et al., 2000) model is used:

$$\overline{\Psi}_{\text{aniso}}\left(\overline{\mathbf{C}}, a_0\right) = \frac{k_1}{2k_2}\left(\exp\left[k_2\left(\overline{I}_4 - 1\right)^2\right] - 1\right), \quad I_4 \geqslant 1, \tag{2}$$

with k_1, and k_2 being material parameters, and I_4 and invariant associated with the vector a, representing the square of the fiber stretch. The invariant I_4 and its deviatoric modified version $\overline{I}_4$ are defined, respectively, as:

$$I_4 = \mathbf{C} : (a \otimes a) \quad ; \quad \overline{I}_4 = \overline{\mathbf{C}} : (a \otimes a)\,, \tag{3}$$

To include the effect of viscosity on the matrix and fibers, the model proposed by Liu et al. (2019) is chosen. In this framework, the deformation gradient, both for the matrix and the fiber, is multiplicatively decomposed into an elastic and a viscous part such that $\mathbf{F} = \mathbf{F}_e^m \mathbf{F}_v^m = \mathbf{F}_e^f \mathbf{F}_v^f$. The free energy function extending the above hyperelastic model is defined as follows:

$$\begin{aligned}\Psi\left(\overline{I}_1, \overline{I}_e, \overline{I}_4, \overline{I}_{4e}, J\right) = {} & \overbrace{\frac{1}{2}\kappa\left(J-1\right)^2 + c\left(\overline{I}_1 - 3\right)}^{\text{Matrix - isotropic - equilibrium}} + \overbrace{\beta_1 c(\overline{I}_e - 3)}^{\text{Matrix - isotropic - viscous}} \\ & + \underbrace{\frac{k_1}{2k_2}\left(\exp\left[k_2\left(\overline{I}_4 - 1\right)^2\right] - 1\right)}_{\text{Fiber - anisotropic - equilibrium}} + \underbrace{\beta_2 \frac{k_1}{2k_2}\left(\exp\left[k_2\left(\overline{I}_{4e} - 1\right)^2\right] - 1\right)}_{\text{Fiber - anisotropic - viscous}},\end{aligned} \tag{4}$$

where κ and c are the elastic parameters from the Neo-Hookean hyperelastic model with the modified invariant $\overline{I}_1 = \mathbf{I} : \overline{\mathbf{C}}$, in which the volumetric part acts as a penalty term, and the parameters β_1 and β_2 are associated to viscosity. In this model, the fibers are considered to work only in tension, hence the expressions related to fibers only contribute by satisfying the conditions $I_4 \geqslant 1$ and $I_{4e} \geqslant 1$. The elastic part of the matrix and fibers invariant, I_e and I_{4e} respectively, with its deviatoric modified form are defined according to the equations 5 and 6. Here, $\mathbf{C}_e^m$ and $\mathbf{C}_v^m$ are the elastic and viscous part of the matrix strain tensor, $\mathbf{C}_e^f$ is the elastic part of the fiber strain tensor, and a_v a viscous unit vector.

$$I_e = I : (\mathbf{C}_e^m)^{-1} = \mathbf{C} : (\mathbf{C}_v^m)^{-1} \quad ; \quad \overline{I}_e = I : \left(\overline{\mathbf{C}}_e^m\right)^{-1} = \overline{\mathbf{C}} : \left(\overline{\mathbf{C}}_v^m\right)^{-1} \tag{5}$$

$$I_{4e} = \mathbf{C}_e^f : (a_v \otimes a_v) \quad ; \quad \overline{I}_{4e} = \overline{\mathbf{C}}_e^f : (a_v \otimes a_v)\,, \tag{6}$$

the explicit equation 4 allows the study of each elastic and viscous part of the wood cell as a composite material and facilitates the numerical implementation in FEniCS.

3 VALIDATION RESULTS

The formulation for a viscoelastic fiber-reinforced composite material described above is implemented in FEniCS finite element (FE) software (Alnæs et al., 2015). In this software, it is necessary to explicitly define the free energy function, so the variational problem is assembled and the displacement field is obtained in each iteration, given a certain geometry, meshing and boundary conditions. For the validation of the model, different numerical examples retrieved from the literature have been taken as references. Following the order presented above, the hyperelastic behavior was first implemented to validate the equilibrium mechanics part of the material and then extended to include viscosity, since the same hyperelastic function is used for the fiber contribution.

For the hyperelastic response, the uniaxial test shown in Figure 2(a) was implemented. It is a discretized unitary cube with a single element whose top face is stretched in the y direction until 1.2, while the other faces are constrained in their displacements. A classical displacement-based FE formulation, based on linear interpolation with Lagrange polynomial is used. The material parameters used can be found in Section 4 of Nolan et al. (2014). In this numerical example, the ratio of the stresses σ_x/σ_y was studied using the HGO model of Eq. 2. Negative results were obtained for certain fiber angles, in particular those closer to the longitudinal direction of stretch, which is unexpected considering the applied tensile stress. Figure 3(a) shows the curves for different fiber inclination angles. The circled curves are the reference results of Nolan et al. (2014), and the continuous curves are the ones obtained using FEniCS. It can be observed that eh hyperelastic model in FEniCS is exactly validated for each fiber angle. A second graph is presented in Figure 3(b), where the results are obtained with the modified version of the HGO model, using the full right Cauchy-Green deformation tensor including the volumetric part. Positive stress results are obtained according to what is expected for a uniaxial tension test.

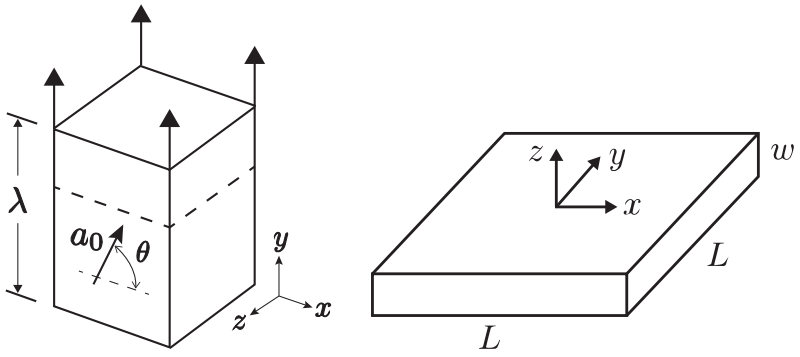

(a) Uniaxial hyperelastic test. (b) Biaxial viscoelastic test.

Figure 2: Numerical test for the model validation. Adapted from Nolan et al. (2014) and Liu et al. (2019), respectively.

With the hyperelastic part of the model validated, the viscosity is included using the free energy function defined in equation 4. For this purpose, the biaxial test of Liu et al. (2019), Figure 2(b), is simulated. The test is a square plate with fibers in the x direction, with displacements applied in the x and y directions for 1 s until a stretch of 1.1 is reached, and then the displacement is kept constant to give place to a relaxation phase of the material. The body was discretized with only one FE using the same previous formulation. The back and bottom faces were constrained to allow bidirectional displacement. The material parameters can be found in Section 5 of Liu et al. (2019).

The implementation of viscoelasticity in finite deformations is not trivial. In this case, two internal variables, C_m^v and I_{4e}, must be updated at each iteration by means of the algorithms described in Liu et al. (2019). A set of non-linear equations should be solved using the the Newton-Raphson method to obtain scalar values that serve to define the invariants I_e and I_{4e}. The results for the relaxation test in the x and y directions are shown in Figures 4(a) and 4(b). The relaxation test results indicate differences in the effect of viscosity, the rate of stress decay

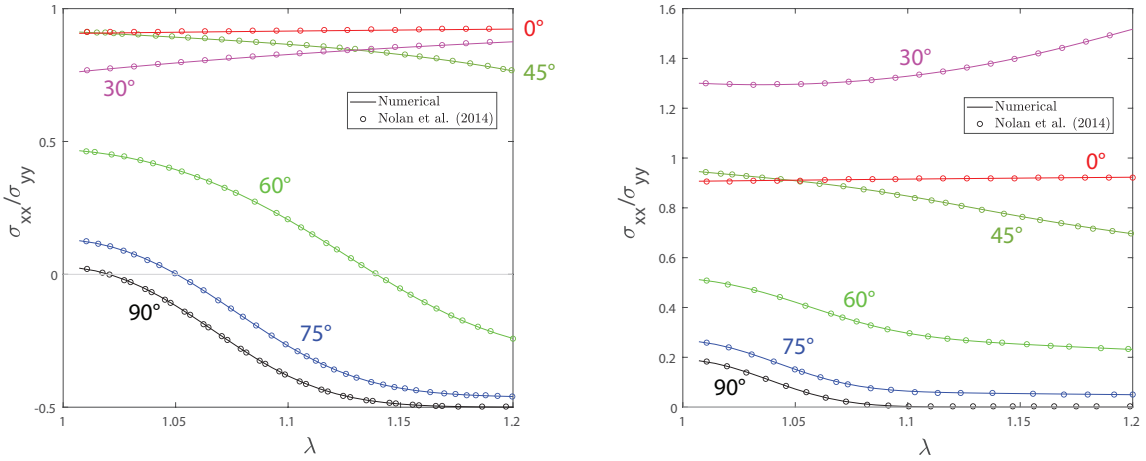

(a) Holzapfel-Gasser-Ogden. (b) Modified Holzapfel-Gasser-Ogden.

Figure 3: Ratio of the Cauchy stress for anisotropic hyperelastic material under uniaxial extension.

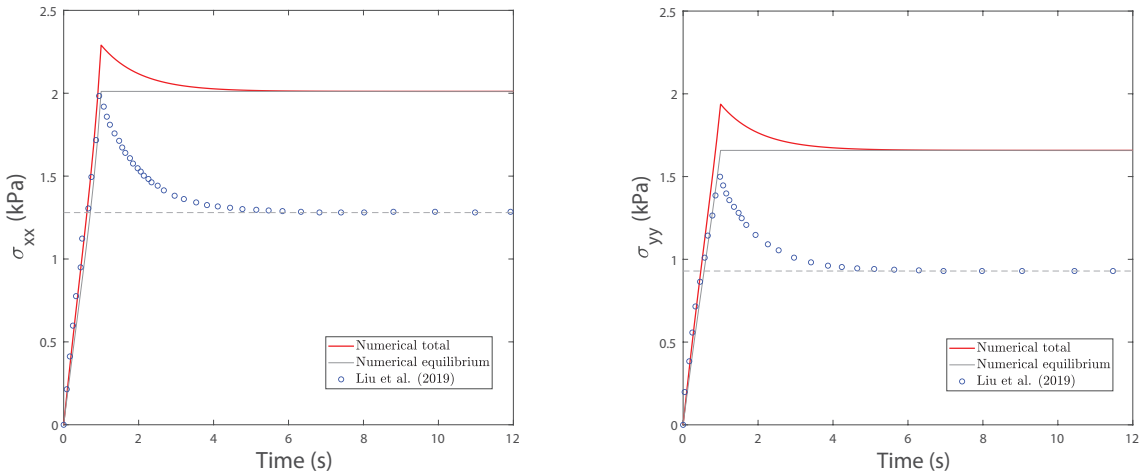

(a) x direction. (b) y direction.

Figure 4: Relaxation results for anisotropic viscoelastic material under biaxial extension.

is lower than the reference values. The elastic part of the material in magnitude is larger, so that the mechanical properties in time also tend to a larger equilibrium. However, the tendency of the numerical curve versus the reference curve in the loading phase gives similar results so that the basics of the numerical model are found to acceptable. In relation to this, Figure 5 shows the evolution of the internal variable C_m^v in x direction, curve that is also delivered in Liu et al. (2019). It is verified that the algorithm that updates this variable is well implemented. Also the values of the invariants I_e and I_{4e} tend to 3 and 1 respectively in the equilibrium state $t \to \infty$, hence it is consistent with the model proposed by Liu et al. (2019).

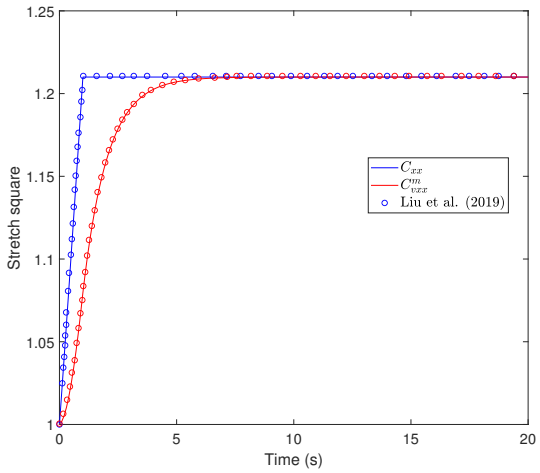

Figure 5: Internal variable evolution for the viscous behavior of the matrix

In general, larger stresses are obtained in the stretching direction when the fiber is at an inclination close to this direction. In Figure 3(b), at an angle of 90° the stress reach its maximum when the fiber is completely vertical. In Figure 4(a), the stresses in the x direction are higher because the fiber is arranged in that direction. This behavior is exactly how the cell wall of wood works in relation to its microfibrils arranged in each sub-layer.

4 CONCLUSIONS

In this work, preliminary results have been presented for the implementation in the FE software FEniCS of a fiber-reinforced composite material with the goal of numerically model the finite viscoelastic mechanical behavior of the wood cell. An anisotropic model originally developed for biomaterials such as arteries has been used. The consistency of the mechanical contribution of the embedded fibers has been tested in relation to their orientation within the material matrix and the expected results when tensile stress is applied. The anisotropic viscoelastic model using FEniCS delivers preliminary results consistent with its internal variables, but it is necessary to improve the FE simulation. After obtaining each displacement, the model proposed by Liu et al. (2019) provides all the necessary information to update the internal variables, and thus the calculation of the stresses can be performed analytically using FEniCS. The next step in this research is to consider a cylindrical geometry as the shape of the cell, and then

include the layers in the thickness in order to characterize the cell wall, as shown in Figure 1. As it is possible to expand the framework to include dissipative behavior, it is also of interest to study the effects of moisture content in the cell, the dimensional changes it produces and how the effects of shrinkage and swelling are coupled with the distribution of microfibrils.

ACKNOWLEDGMENTS

C.F. Guzmán acknowledges the financial support from the Chilean National Agency for Research and Development (ANID), Fondecyt research project No. 11200638.

References

Alnæs, M., J. Blechta, J. Hake, A. Johansson, B. Kehlet, A. Logg, C. Richardson, J. Ring, M. E. Rognes, and G. N. Wells (Dec. 2015). "The FEniCS Project Version 1.5". In: *Archive of Numerical Software* 3.100.

Dinwoodie, J. M. (Feb. 2000). *Timber: Its Nature and Behaviour*. London ; New York : England.

Holzapfel, G. A., T. C. Gasser, and R. W. Ogden (July 2000). "A New Constitutive Framework for Arterial Wall Mechanics and a Comparative Study of Material Models". In: *Journal of elasticity and the physical science of solids* 61.1, pp. 1–48.

Liu, H., G. A. Holzapfel, B. H. Skallerud, and V. Prot (Mar. 2019). "Anisotropic Finite Strain Viscoelasticity: Constitutive Modeling and Finite Element Implementation". In: *Journal of the Mechanics and Physics of Solids* 124, pp. 172–188.

Nolan, D. R., A. L. Gower, M. Destrade, R. W. Ogden, and J. P. McGarry (Nov. 2014). "A Robust Anisotropic Hyperelastic Formulation for the Modelling of Soft Tissue". In: *Journal of the Mechanical Behavior of Biomedical Materials* 39, pp. 48–60.